Materials Letters 330 (2023) 133274

Contents lists available at ScienceDirect

Materials Letters

journal homepage: www.elsevier.com/locate/matlet

High-temperature superelasticity and shape memory effect in [0 1 1]$_{B2}$-oriented single crystals of the $(TiZrHf)_{50}Ni_{25}Cu_{15}Co_{10}$ high-entropy alloy

Y.I. Chumlyakov, I.V. Kireeva *, L.P. Yakovleva, A.V. Vyrodova, I.V. Kuksgauzen

National Research Tomsk State University, Tomsk 634050, Russia

ARTICLE INFO

Keywords:
$(TiZrHf)_{50}Ni_{25}Cu_{15}Co_{10}$ high-entropy alloy
Single crystals
High-temperature superelasticity
Shape memory effect

ABSTRACT

Superelasticity (SE) and shape memory effect (SME) of [0 1 1]$_{B2}$-oriented single crystals in B2-phase of the $(TiZrHf)_{50}Ni_{25}Cu_{15}Co_{10}$ high-entropy alloy (at.%), with B2-B19′ martensitic transformation, have been studied in the post-growth state under compression. It is shown that SE is observed within a wide temperature range of T = M_s = 404 K to 528 K. The maximum SE value is 4.4 %, and the SME reaches 4.3–4.7 %.

1. Introduction

High-temperature shape memory alloys are alloys that exhibit shape memory effect (SME) and superelasticity (SE) at temperatures above 373 K [1]. Such alloys, with high-temperature shape memory, are widely used in aviation and astronautics. An increase in the temperatures of martensitic transformation (MT) in TiNi alloys is achieved by alloying with a third element, for instance, Zr, Hf, Pd, Au, Co, Cu [2]. Recently, new TiZrHfNiCoCu high-entropy alloys (HEAs) have been proposed, in which Ti is partially replaced by Zr and Hf, and Ni is partially replaced by Co and Cu [3,4]. These alloys experience reversible thermoelastic B2-B19′ MT and exhibit high-temperature SME and SE. The development of SE at high T ≥ 373–523 K in HEAs is facilitated by two impotent points: i) the difficulty of diffusion of vacancies and ii) strong hardening of the high-temperature B2-phase due to precipitation of particles of secondary phases during high-temperature tests and heavy lattice distortion [5,6].

In the present paper, on [0 1 1]$_{B2}$-oriented crystals in B2-phase of the $(TiZrHf)_{50}Ni_{25}Cu_{15}Co_{10}$ (at.%) HEA in the post-growth state, we set the task of studying the stress-induced B2-B19′ MT, SE and SME under compression. Firstly, there are still no works in the literature on the MT studies of these HEAs using single crystals. Secondly, single crystals make it possible to exclude the influence of grain boundaries on the development of B2-B19′ MT at the high test temperatures T ≥ 473–573 K and a high stress level on the development of stress-induced MT at σ ≥ 800–1200 MPa. Thirdly, [0 1 1]$_{B2}$ orientation was chosen due to the maximum value of the theoretical lattice deformation ε_0 = 5.15 % for B2-B19′ MT in TiNi alloys under compression [2,7]. In this orientation, the ε_0 value is determined only by the ε_{CVP} (ε_{CVP} is deformation of twin-related correspondence variants pairs which form habit planes) due to the zero deformation for the detwinning ε_{det} of B19′-martensite under compression [2,7].

2. Materials and methods

Alloy ingots with a nominal composition of $(TiZrHf)_{50}Ni_{25}Cu_{15}Co_{10}$ (at.%) for crystal growth were remelted seven times in an ARC-200 electric arc furnace from pure-elements in a helium atmosphere. Single crystals were grown by the Bridgman method in a graphite crucibles and helium atmosphere. Crystal orientation was determined using DRON-3 M X-ray diffractometer. To determine the [0 1 1]$_{B2}$ orientation in B2-phase, the crystals were heated to temperature of 450 K in a goniometer in a special heated holder. Samples for compression had dimensions of 6x3x3 mm^3 with [0 1 1] orientation along the maximum size of 6 mm. Start M_s and finish M_f temperatures of the forward B2-B19′ MT during cooling and start A_s and finish A_f temperatures of the reverse B19′-B2 MT during heating, were determined by the intersection of tangents on the temperature dependence of the electrical resistance ρ(T). The temperature range of the stress-induced MT and the temperature dependence of the SE were investigated using an Instron 5969 universal testing machine at the deformation rate of $4 \bullet 10^{-4}$ s^{-1}. The SME was determined by two methods. In the case of first method, SME was studied on home-made dilatometer in cooling/heating in the temperature range from 77 to 400 K, at a constant stress in the cycle, with a

* Corresponding author.

https://doi.org/10.1016/j.matlet.2022.133274
Received 2 August 2022; Received in revised form 12 September 2022; Accepted 28 September 2022
Available online 3 October 2022

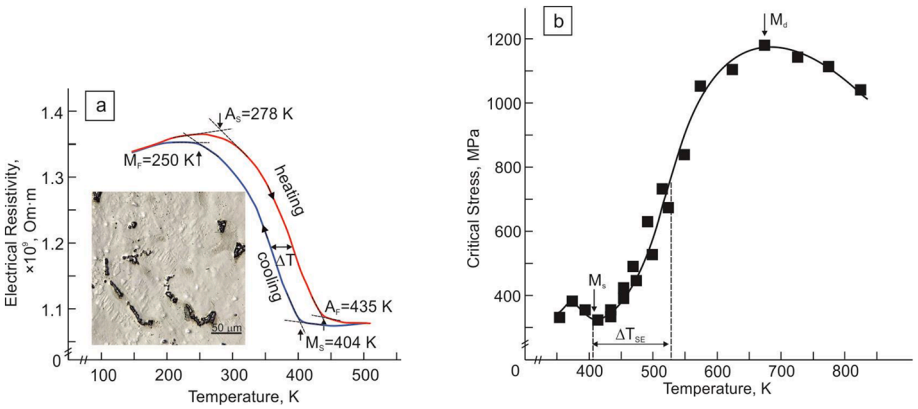

Fig. 1. Temperature dependence of ρ(T) (a) and Temperature dependence of the critical stresses under compression (b) of $[0\ 1\ 1]_{B2}$-oriented $(TiZrHf)_{50}Ni_{25}Cu_{15}Co_{10}$ HEA crystals in the post-growth state. Insert to Fig. 1a optical image of the crystal surface in the post-growth state.

heating/cooling rate of 10 K/min. In the case of second method, the crystal was deformed at $T < M_s$ and then heated in furnace at $T > A_f$. Heating of a part of the samples preliminarily deformed at $T < M_s$ was carried out in a dilatometer, and the dependence of the reversible strain ε_{rev} on the test temperature was recorded. To determine the alloying elements a scanning electron microscope (SEM) TESCAN VEGA3 with an energy dispersive spectroscopy detector was used. The surfaces of samples in the post-growth state were examined in a KEYENCE VHX-2000 optical microscope.

3. Results and discussion

In the post-growth state, single crystals are characterized by a two-phase structure. Large particles are observed on the sample surface (Fig. 1a, Inset). Single crystals in the initial state after growth in the free-particle areas had the following composition: Ti = 16.16 at.%, Zr = 14.37 at.%, Hf = 19.0 at.%, Ni = 25.7 at.%, Cu = 14.14 at.%, Co = 10.63 at.%, which did not differ much from the nominal composition of the alloy ingots. The particles had a chemical composition: Co = 3.9 at.%, Cu = 7.04 at.%, Ni = 12.1 at.%, Ti = 16.17 at.%, Zr = 25.12 at.%, Hf = 24.48 at.%, C = 8.15 at.%, O = 3.04 at.%. The difference between the content of (TiZnHf) and (NiCoCuCO) was close to a ratio of 2:1. Consequently, these particles are close in composition to the Ti_2Ni phase stabilized by C (carbon) and O (oxygen) atoms. It is assumed that oxygen can be contained in the surface layer of pure metals. Carbon atoms enter the alloy during the growth of single crystals in graphite crucibles. The particles have a size along the length of 25–35 μm on average, and their volume fraction does not exceed 1 %, and they do not contribute to the strength properties of the high-temperature B2-phase [8,9].

The B2-B19′ MT is characterized by the following MT temperatures: M_s = 404K, M_f = 250 K, A_s = 278 K, A_f = 435 K. Therefore, the $(TiZrHf)_{50}Ni_{25}Cu_{15}Co_{10}$ HEA single crystals are a high-temperature shape memory crystals with a narrow temperature hysteresis $\Delta T_h = A_f – M_s$ = 31 K (Fig. 1a). The temperature dependence of the critical stresses σ_{cr} on temperature T (σ_{cr}(T)) has a form characteristic of alloys undergoing MT under stress (Fig. 1b) [2]. The minimum stress σ_{cr} is observed at the M_s temperature, which coincides with M_s determined from ρ(T) curve (Fig. 1a). At $T < M_s$, the σ_{cr}(T) is related to the reorientation of the cooling martensite [2,10]. The maximum stress σ_{cr} on the σ_{cr}(T) dependence is reached at M_d temperature, at which the stresses of the onset of stress-induced MT, σ_{cr}(SIM), are equal to the stresses of the beginning of plastic deformation of B2-phase, σ_{cr}(B2). At $T = M_d$, the σ_{cr}(B2) = 1180 MPa and, consequently, crystals are high-strength crystals. It is interesting that $\sigma_{cr}(M_s)$ = 300 MPa also turn out to be high in comparison with TiNi alloys [2,10]. Such high values of $\sigma_{cr}(M_s)$ and σ_{cr}(B2) are due to significant solid solution hardening in the $(TiZrHf)_{50}Ni_{25}Cu_{15}Co_{10}$ HEA crystals [5,6]. In the temperature range

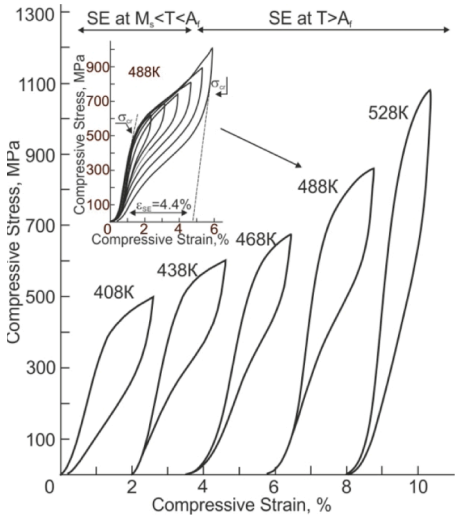

Fig. 2. Temperature range of superelasticity in $[0\ 1\ 1]_{B2}$-oriented crystals of the $(TiZrHf)_{50}Ni_{25}Cu_{15}Co_{10}$ HEA under compression. The insert shows the maximum SE.

from M_s to T = 575 K, a stage associated with stress-induced MT is observed, which is described by the Clapeyron-Clausius relation [2]:

$$\frac{d\sigma_{cr}(SIM)}{dT} = -\frac{\Delta S}{\varepsilon_0} = -\frac{\Delta H}{T_0\varepsilon_0} \quad (1)$$

where ΔH, ΔS are the change in enthalpy and entropy at B2-B19′ MT, T_0 is the phase equilibrium temperature, ε_0 is the lattice deformation. The value of $\alpha = d\sigma_{cr}(SIM)/dT$ = 5.2 MPa/K is close to that previously found for the [0 1 1]-oriented TiNi crystals under compression [10].

Under compression, in the $[0\ 1\ 1]_{B2}$-oriented $(TiZrHf)_{50}Ni_{25}Cu_{15}Co_{10}$ HEA crystals, SE is observed within a wide temperature range from $T = M_s$ = 404 K to T = 528 K (Fig. 2). Comparison of the temperature range of reversible strain with MT temperatures shows the following (Fig. 1a, 2). Firstly, SE takes place in the temperature range $M_s < T < A_f$, as at $T > A_f$, when B19′-martensite becomes thermodynamically unstable [2,11]. Secondly, SE is observed at $T > A_f$ = 435 K. Thus, the $[0\ 1\ 1]_{B2}$-oriented $(TiZrHf)_{50}Ni_{25}Cu_{15}Co_{10}$ HEA crystals demonstrate high-temperature SE.

In the "load-unloading" cycle, the maximum SE was obtained at 488 K (Fig. 2, Insert). At 488 K, the maximum SE is equal to 4.4 %, which is close to the ε_0 = 5.15 % [2,7] and experimental data of the $[0\ 1\ 1]_{B2}$-oriented TiNi crystals [7]. MT develops with high transformation hardening coefficient $\Theta = d\sigma/d\varepsilon$ = 9.6 GPa. With an increase in the

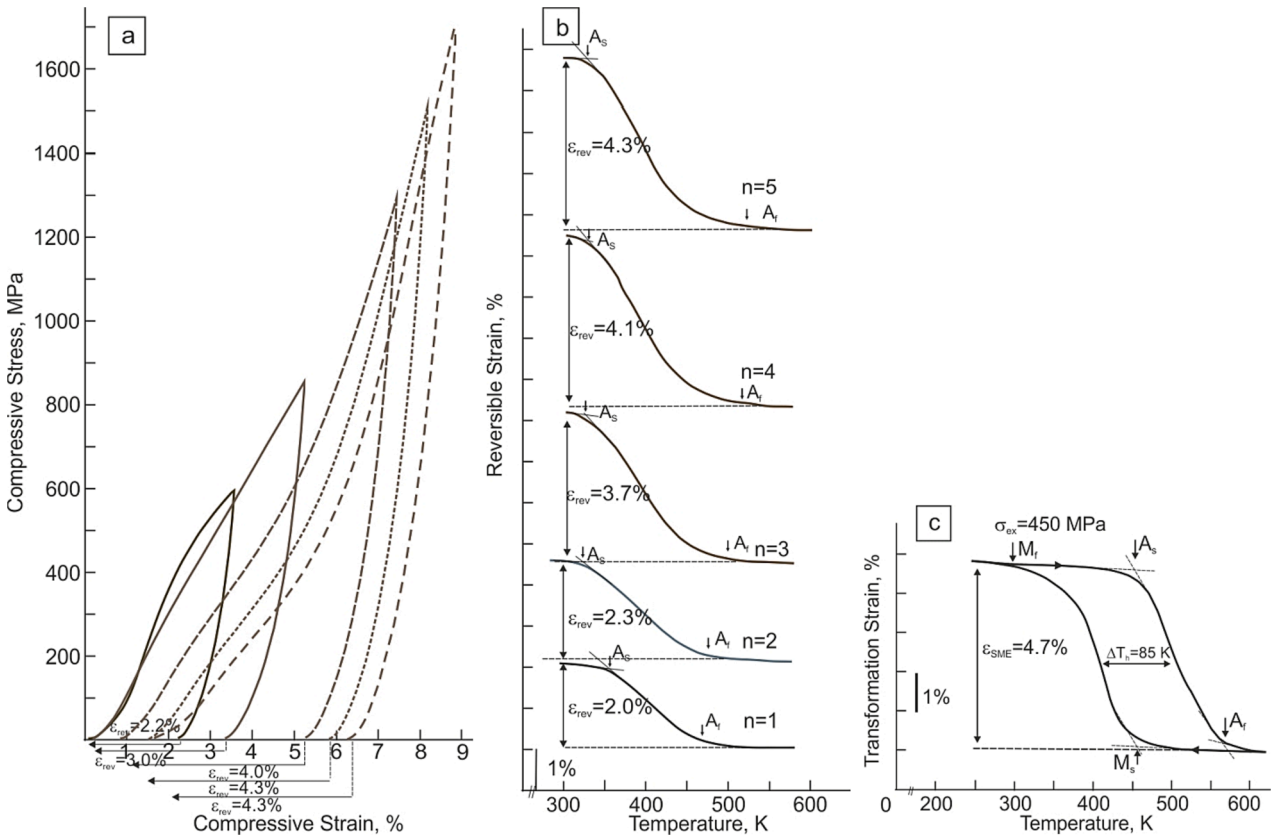

Fig. 3. Shape memory effect in $[0\ 1\ 1]_{B2}$-oriented crystals of the $(TiZrHf)_{50}Ni_{25}Cu_{15}Co_{10}$ HEA under compression: (a) - deformation at 296 K and then heated in furnace in free state; (b) - deformation as in case (a) at 296 K and heating in a dilatometer without stress; (c) - shape memory effect at compressive stress of 450 MPa.

strain level in cycle, an increase in mechanical hysteresis $\Delta\sigma$ is observed, the value of which is determined at half of the SE loop. At all studied temperatures, the SE curves have a characteristic "cigar-like" shape without a plateau. This shape of "stress–strain" curve indicates a significant contribution to the transformation hardening of the elastic energy ΔG_{el}, which increases with a growth in the volume fraction of martensite.

The SME studies are presented on Fig. 3. The crystals were deformed by strain of ε_1 at 296 K and then heated in furnace or in a dilatometer without stress (Fig. 3a and 3b). After heating, the reversible strain ε_2 was measured. If $\varepsilon_1 = \varepsilon_2$, then the complete return of the strain is realized, at which the irreversible deformation $\varepsilon_{ir} = 0$. Therefore, there is a SME. With a successive increase in ε_1 in the "stress–strain" cycle, the maximum value of $\varepsilon_2 = 4.3$ % or SME was obtained, which was close to the SE value. The maximum SME 4.7 % were obtained during cooling/heating under an external compressive stress $\sigma_{ex} = 450$ MPa (Fig. 3c). In $(TiZrHf)_{50}Ni_{25}Cu_{15}Co_{10}$ polycrystals, SE and SME were 3.5 and 4.5 %, respectively, at three-point bending, which was close to those for single crystals in post-growth state [8]. It is interesting that $A_s \leq M_s$ (Fig. 3c). According to the thermodynamic analysis of the development of thermoelastic MT, this means that the elastic energy ΔG_{el} stored during MT exceeds the double value of the dissipated energy ΔG_{dis}, $\Delta G_{el} > 2\Delta G_{dis}$ [2]. The SE curves also show that the stress σ_{cr} of the onset of the forward stress-induced MT, for instance, at T = 488 K, is less than the stress σ_{cr} of the onset of the reverse MT upon unloading (Fig. 2, Insert). This is also associated with the accumulation of a large elastic energy ΔG_{el}, which significantly exceeds ΔG_{dis}, $\Delta G_{el} \geq (4–6)\Delta G_{dis}$ [11]. The development of the reversible B2-B19' MT within the temperature range of M_s to A_f is associated with a high ratio of $\Delta G_{el}/\Delta G_{dis} \geq 4–6$ [11]. Previously, SE in this temperature range was observed in the [0 0 1]-oriented FeNiCoAlNb HEA crystals and a thermodynamic analysis of this problem was proposed [11].

4. Conclusions

For the first time, single crystals of the $(TiZrHf)_{50}Ni_{25}Cu_{15}Co_{10}$ (at. %) HEA are grown, which in the post-growth state are characterized by a high $M_s = 404$ K temperature. In the $[0\ 1\ 1]_{B2}$-oriented crystals under compression, SE is observed within a wide temperature range of $M_s = 404$ K to T = 528 K. The maximum SE value of 4.4 % was observed at 488 K. The shape memory effect is equal to 4.3–4.7 %. The resulting $(TiZrHf)_{50}Ni_{25}Cu_{15}Co_{10}$ HEA single crystals are high-strength functional materials with high-temperature SE.

CRediT authorship contribution statement

Y.I. Chumlyakov: Conceptualization, Supervision, Project administration, Funding acquisition. **I.V. Kireeva:** Supervision, Investigation, Writing – original draft, Writing – review & editing. **L.P. Yakovleva:** Investigation. **A.V. Vyrodova:** Investigation. **I.V. Kuksgauzen:** Investigation.

Declaration of Competing Interest

The authors declare that they have no known competing financial interests or personal relationships that could have appeared to influence the work reported in this paper.

Data availability

Data will be made available on request.

Acknowledgment

This study has been funded by the Russian Science Foundation, Grant

No. 22-19-00017.

References

[1] J. Ma, I. Karaman, R.D. Noebe, Int. Mater. Rev. 55 (2010) 257–315.
[2] K. Otsuka, X. Ren, Prog. Mater Sci. 50 (2005) 511–678.
[3] G.S. Firstov, T.A. Kosorukova, Y.N. Koval, V.V. Odnosum, Mater. Today:. Proc. 2 (3) (2015) S499–S503.
[4] C.H. Chen, Y.J. Chen, Scr. Mater. 162 (2019) 185–189.
[5] J.W. Yeh, S.K. Chen, S.J. Lin, J.Y. Gan, T.S. Chin, T.T. Shun, C.H. Tsau, S.Y. Chang, Adv. Eng. Mater. 6 (2004) 299–303.
[6] K.Y. Tsai, M.H. Tsai, J.W. Yeh, Acta Mater. 61 (2013) 4887–4897.
[7] H. Sehitoglu, R. Hamilton, D. Canadinc, X.Y. Zhang, K. Gall, I. Karaman, Y. Chumlyakov, H.J. Maier, Metall. Mat. Trans. A. 34 (5) (2003) 6–13.
[8] H.-C. Lee, Y.-J. Chen, C.-H. Chen, Entropy 21 (2019) 1027.
[9] I.U. Rehman, S. Li, T.-H. Nam, J. Alloy. Compd. 884 (2021), 161108.
[10] I.V. Kireeva, Y.I. Chumlyakov, A.V. Vyrodova, Z.V. Pobedennaya, E.S. Marchenko, Mater. Lett. 324 (2022), 132817.
[11] Y.I. Chumlyakov, I.V. Kireeva, Z.V. Pobedennaya, P. Kroos, T. Niendorf, J. Alloy. Compd. 856 (2020), 158158.